bioRxiv preprint doi: https://doi.org/10.1101/256958; this version posted July 6, 2018. The copyright holder for this preprint (which was not certified by peer review) is the author/funder. All rights reserved. No reuse allowed without permission.

Biological Sciences: Biochemistry

Multiple prebiotic metals mediate translation

Marcus S. Bray[a*], Tim K. Lenz[b*], Jessica C. Bowman[b], Anton S. Petrov[b], Amit R. Reddi[b], Nicholas V. Hud[b], Loren Dean Williams[b,1] and Jennifer B. Glass[c,1]

[a]School of Biological Sciences, Georgia Institute of Technology, 950 Atlantic Dr, Atlanta, GA, USA, 30332

[b]School of Chemistry and Biochemistry, Georgia Institute of Technology, 901 Atlantic Dr, Atlanta GA, USA, 30332

[c]School of Earth and Atmospheric Sciences, Georgia Institute of Technology, 311 Ferst Dr, Atlanta, GA, US, 30332

[*]These two people have contributed equally to this work.

[1]To whom correspondence should be addressed:
Jennifer B. Glass: School of Earth & Atmospheric Sciences, Georgia Institute of Technology, Atlanta, GA 30332; jennifer.glass@eas.gatech.edu; Tel. 404- 894-3942; Fax. 404-894-5638
Loren Dean Williams: School of Chemistry & Biochemistry, Georgia Institute of Technology, Atlanta, GA 30332; loren.williams@chemistry.gatech.edu; Tel. 404-385-6258; Fax. 404-894-2295

Keywords: Translation, SHAPE, iron, manganese, magnesium, ribosome, ribosome function, ribosome structure, protein synthesis

Running title: Multiple prebiotic metals mediate translation

bioRxiv preprint doi: https://doi.org/10.1101/256958; this version posted July 6, 2018. The copyright holder for this preprint (which was not certified by peer review) is the author/funder. All rights reserved. No reuse allowed without permission.

ABSTRACT

Today, Mg^{2+} is an essential cofactor with diverse structural and functional roles in life's oldest macromolecular machine, the translation system. We tested whether ancient Earth conditions (low O_2, high Fe^{2+}, high Mn^{2+}) can revert the ribosome to a functional ancestral state. First, SHAPE (Selective 2'-Hydroxyl Acylation analyzed by Primer Extension) was used to compare the effect of Mg^{2+} vs. Fe^{2+} on the tertiary structure of rRNA. Then, we used *in vitro* translation reactions to test whether Fe^{2+} or Mn^{2+} could mediate protein production, and quantified ribosomal metal content. We found that: (i) Fe^{2+} and Mg^{2+} had strikingly similar effects on rRNA folding; (ii) Fe^{2+} and Mn^{2+} can replace Mg^{2+} as the dominant divalent cation during translation of mRNA to functional protein; (iii) Fe^{2+} and Mn^{2+} associated extensively with the ribosome. Given that the translation system originated and matured when Fe^{2+} and Mn^{2+} were abundant, these findings suggest that Fe^{2+} and Mn^{2+} played a role in early ribosomal evolution.

SIGNIFICANCE

Ribosomes are found in every living organism where they are responsible for the translation of messenger RNA into protein. The ribosome's centrality to cell function is underscored by its evolutionary conservation; the core structure has changed little since its inception ~4 billion years ago when ecosystems were anoxic and metal-rich. The ribosome is a model system for the study of bioinorganic chemistry, owing to the many highly coordinated divalent metal cations that are essential to its function. We studied the structure, function, and cation content of the ribosome under early Earth conditions (low O_2, high Fe^{2+}, high Mn^{2+}). Our results expand the roles of Fe^{2+} and Mn^{2+} in ancient and extant biochemistry as a cofactor for ribosomal structure and function.

bioRxiv preprint doi: https://doi.org/10.1101/256958; this version posted July 6, 2018. The copyright holder for this preprint (which was not certified by peer review) is the author/funder. All rights reserved. No reuse allowed without permission.

\body

Life arose around 4 billion years ago on an anoxic Earth with abundant Fe^{2+} and Mn^{2+}, which would have maintained solubility in the absence of O_2 (1-5). Biochemistry had access to these metals for over a billion years before biological O_2 production was sufficient to oxidize and precipitate them. The pervasive use of these "prebiotic" metals in extant biochemistry, despite barriers to their biological acquisition, likely stems from their importance in the evolution of the early biochemical systems.

The translation system, which synthesizes all coded protein (6), originated and matured during the Archean Eon (4-2.5 Ga) in low-O_2, high-Fe^{2+}, and high-Mn^{2+} conditions (7). The common core of the ribosome, and many other aspects of the translation system, have remained essentially frozen since the last universal common ancestor (8). In extant biochemistry, Mg^{2+} ions are essential for both structure and function of the ribosome (9) and other enzymes involved in translation (10). In ribosomes, Mg^{2+} ions are observed in a variety of structural roles (**Table 1**), including in Mg^{2+}-rRNA clamps (11, 12) (**Fig. 1a**), in dinuclear microclusters that frame the peptidyl transferase center (PTC) (12) (**Fig. 1b**), and at the small subunit-large subunit (SSU-LSU) interface (13) (**Fig. 1c**). Functional Mg^{2+} ions stabilize a critical bend in mRNA between the P-site and A-site codons (14) (**Fig. 1d**), and mediate rRNA-tRNA and rRNA-mRNA interactions (15) (**Fig. 1e, f**). Accessory enzymes needed for translation – aminoacyl tRNA synthetases, methionyl-tRNA transformylase, creatine kinase, myokinase, and nucleoside-diphosphate kinase – also require Mg^{2+} ions as cofactors (**Table 1**).

There is abundant evidence that multiple types of cationic species can interact productively with various RNAs (16-18). Recent results support a model in which Fe^{2+} and Mn^{2+}, along with Mg^{2+}, were critical cofactors for ancient nucleic acid function. As predicted by this model, functional Mg^{2+}-to-Fe^{2+} substitutions under anoxic conditions were experimentally verified to support RNA folding and catalysis by ribozymes (19, 20), a DNA polymerase, a DNA ligase, and an RNA polymerase (21). Functional Mg^{2+}-to-Mn^{2+} substitution has long been known for DNA polymerase (21-23). In contrast to Mg^{2+}, Fe^{2+} has been shown to more effectively 'activate' RNA. The phosphate affinity of Fe^{2+}, because of the lower energies of its d-orbitals, is slightly greater than that of Mg^{2+}. In first shell coordination complexes, the proximal phosphorus shows greater electron depletion and enhanced susceptibility to nucleophilic attack. Therefore, for at least some nucleic acid processing enzymes, optimal activity is observed at lower concentrations of Fe^{2+} than Mg^{2+} (19, 21).

Based on these previous results, we hypothesized that Fe^{2+} and Mn^{2+} could partially or fully replace Mg^{2+} in the ribosome during translation. In this study, we relocated the translation system to the low-O_2, high-Fe^{2+}, and high-Mn^{2+} environment of its ancient roots, and compared its structure, function, and cation content under modern vs. ancient conditions.

Results

Fe^{2+} folds LSU rRNA to a near-native state. To test whether Fe^{2+} can substitute for Mg^{2+} in folding rRNA to a native-like state, we compared LSU rRNA folding in the presence of Fe^{2+} or Mg^{2+} by SHAPE (Selective 2'-Hydroxyl Acylation analyzed by Primer Extension). SHAPE provides quantitative, nucleotide resolution information about flexibility, base pairing and 3D structure, and has previously been used to monitor the influence of cations, small molecules, or proteins on RNA structure (24-28). We previously used SHAPE to show that the LSU rRNA adopts a near-native state in the presence of Mg^{2+}, with the core inter-domain architecture of the assembled ribosome and residues positioned for interactions with rProteins (29). In this study, SHAPE experiments were performed in an anoxic chamber to maintain the oxidation state and solubility of Fe^{2+}. The minimum concentration required to fully fold rRNA, 2.5 mM Fe^{2+} or 10 mM Mg^{2+}, was used for all SHAPE experiments (**Additional Data Table S1**).

bioRxiv preprint doi: https://doi.org/10.1101/256958; this version posted July 6, 2018. The copyright holder for this preprint (which was not certified by peer review) is the author/funder. All rights reserved. No reuse allowed without permission.

Addition of Fe^{2+} or Mg^{2+} induced widespread structural changes in the Na^{+}-form LSU rRNA, reflected in SHAPE reactivity as ΔFe^{2+} or ΔMg^{2+} (see **Materials and Methods**) and displayed as 'heat maps' on the LSU rRNA secondary structure (**Fig. 2**). The ΔFe^{2+} and ΔMg^{2+} heat maps were broadly similar at the nucleotide and regional scales (**Fig. 2d**, **e)**, indicating similar effects of Fe^{2+} or Mg^{2+} on rRNA folding. Helical regions tended to be invariant, whereas rRNA loops and bulges were impacted by addition of Fe^{2+} or Mg^{2+}. Of the sites that exhibited a significant response (>0.3 SHAPE units) to Mg^{2+}, 86% of nucleotides (43/50) exhibited a similar trend with Fe^{2+}. The greatest discrepancy between Fe^{2+} and Mg^{2+} is observed in the L11 binding domain (**Fig. 2d, e**).

Fe^{2+} and Mn^{2+} mediate translation. Translation reactions were performed in an anoxic chamber in the presence of different divalent cations and cation concentrations. Production of the protein dihydrofolate reductase (DHFR) from its mRNA was used to monitor translational activity. Protein synthesis was assayed by measuring the rate of NADPH oxidation by DHFR. These reactions were conducted in a small background of 2.5 mM Mg^{2+} (**Fig. S1a**). This background is below the requirement to support translation, consistent with previous findings that a minimum of ~5 mM Mg^{2+} is needed for assembly of mRNA onto the SSU (30-32). As a control, we recapitulated the previously established Mg^{2+} dependence of the translation system, and then repeated the assay with Fe^{2+}.

The activity profile of the translation system with varied Fe^{2+} closely tracked the profile with varied Mg^{2+} (**Fig. 3**). Below 7.5 mM total divalent cation concentration, minimal translation occurred with either Fe^{2+} or Mg^{2+}, as observed elsewhere (33). Activity peaked at 9.5 mM for both cations and decreased modestly beyond the optimum. At a given divalent cation concentration, Fe^{2+} supported around 50-80% of activity with Mg^{2+}. This result was observed with translation reactions run for 15, 30, 45, 60, 90 and 120 min with optimal divalent cation concentrations (**Fig. 4**). Along with Mg^{2+} and Fe^{2+}, we investigated the abilities of other divalent cations to support translation, including Mn^{2+}, Co^{2+}, Cu^{2+}, and Zn^{2+}. We found that Mn^{2+} supported translation at levels similar to Fe^{2+}, whereas no activity was detected with Co^{2+}, Cu^{2+}, or Zn^{2+} (**Fig. S2**).

To test whether alternative divalent cations could completely replace Mg^{2+} in translation, we decreased the background Mg^{2+} from 2.5 to 1 mM by thoroughly washing the ribosomes prior to translation reactions with 7-11 mM Fe^{2+} or Mn^{2+} (**Fig. S1b**). With 1 mM background Mg^{2+}, Fe^{2+} supported 12-23% of the activity with Mg^{2+} over the concentrations tested, while Mn^{2+} supported 43-50% activity relative to Mg^{2+} (**Fig. 5a**). Washing the factor mix allowed us to decrease the background Mg^{2+} in translation reactions to ~4-6 μM (**Fig. S1c**). At this level, minimal protein production was observed with Fe^{2+}, while Mn^{2+} supported 29-38% of the activity measured with Mg^{2+} (**Fig. 5b**).

Fe^{2+} and Mn^{2+} associate extensively with the ribosome. To experimentally confirm that Fe^{2+} and Mn^{2+} associate with the assembled ribosome, we analyzed the Fe^{2+} and Mn^{2+} content of ribosomes after incubation in anoxic reaction buffer containing 7 mM Fe^{2+} or 7 mM Mn^{2+}. Under the conditions of our translation reactions, 584 ± 9 Fe^{2+} ions or 507 ± 28 Mn^{2+} ions associate with each ribosome.

Finally, we computationally investigated whether Mg^{2+}, Fe^{2+}, and Mn^{2+} might be interchangeable during translation using quantum mechanical characterization of M^{2+}-rRNA clamps, which are frequent in the ribosome (11, 12) **(Fig. 1a, S3).** The geometries of Fe^{2+}-rRNA clamps and Mg^{2+}-rRNA clamps are nearly identical (**Table S1**). However, due to the accessibility of its d-orbitals, more charge is transferred to Fe^{2+} (**Table S2**), leading to greater stability of Fe^{2+}-rRNA vs. Mg^{2+}-rRNA clamps **(Table S3)**. The effect of the modestly greater radius of Mn^{2+} (**Table S1)** is offset by d-orbital charge transfer **(Table S2)**, leading to comparable stabilities of Mg^{2+}-rRNA and Mn^{2+}-rRNA clamps (**Table S3).**

Discussion

bioRxiv preprint doi: https://doi.org/10.1101/256958; this version posted July 6, 2018. The copyright holder for this preprint (which was not certified by peer review) is the author/funder. All rights reserved. No reuse allowed without permission.

In this study, we successfully replaced ribosomal Mg^{2+} with Fe^{2+} or Mn^{2+} under conditions mimicking the anoxic Archean Earth. Previously, the only cation known to mediate rRNA folding and function of the translation system was Mg^{2+}. We found that rRNA folds to the same extent, and to essentially the same global state (34, 35), with Fe^{2+} or Mg^{2+} under anoxia. The minimum concentration of Fe^{2+} required to fold the rRNA is 4-fold less than the requisite Mg^{2+} concentration. We showed that Fe^{2+} or Mn^{2+} can serve as the dominant divalent cation during translation. Background Mg^{2+} as high as 2.5 mM was insufficient to mediate protein synthesis, and at least 5 mM additional Mg^{2+}, Fe^{2+}, or Mn^{2+} was required to restore translational activity. Further, we demonstrated that Mn^{2+} can mediate translation in place of Mg^{2+}, suggesting that Mn^{2+} can mediate each of the M^{2+}-RNA interactions in **Fig. 1**. These findings suggest that functional Mg^{2+}-Mn^{2+} and Mg^{2+}-Fe^{2+} substitutions can occur in large ribozymes, similar to previous reports for protein enzymes and small ribozymes (21-23, 36, 37). Near-complete removal of Mg^{2+} prevented Fe^{2+}-mediated translation and partially inhibited Mn^{2+}-mediated translation, suggesting that Mg^{2+} is optimal for some specific roles in the translation system. Regardless, the general effectiveness of Mg^{2+}-Mn^{2+} and Mg^{2+}-Fe^{2+} substitutions in the translation system is astounding considering the enormous number of divalent cations associated with a given ribosome, and the diversity of their structural and functional roles (9, 10) (**Table 1, Fig. 1**).

The observation that >500 Fe^{2+} or Mn^{2+} ions can associate with a ribosome is consistent with the extent of Mg^{2+} association observed by x-ray diffraction (100-1000 Mg^{2+} per ribosome (38)), and supports a model in which Fe^{2+} or Mn^{2+} has replaced Mg^{2+} as the dominant divalent cation in our experiments. The high capacity of ribosomes for Fe^{2+} and Mn^{2+} reflects all ribosome-associated ions, including condensed, glassy and chelated divalent cations (39), and possibly also ions associated with ribosomal proteins, such as those previously shown to bind Zn^{2+} (e.g. S2, S15, S16, S17, L2, L13, L31, L36 in *E. coli*) (40).

The differences in protein production observed among the three divalent cations in this study arise from a variety of evolutionary, and physiological factors. For instance, *E. coli* may be evolutionarily adapted to use Mg^{2+} instead of Fe^{2+} or Mn^{2+} in ribosomes. The difference in translational activity between Mn^{2+} and Fe^{2+}, particularly when background Mg^{2+} was removed, suggests that Mn^{2+} is more viable upon full substitution. Such Mn^{2+}/Mg^{2+} interchangeability may result from the comparable stabilities of Mn^{2+} and Mg^{2+} in M^{2+}-rRNA clamps (**Fig. S3**). An additional contribution to the lower net effectiveness of Fe^{2+} in translation may be due to its higher redox activity; indeed, Fe^{2+}-mediated oxidative damage to RNA has been observed in ribosomes purified from Alzheimer hippocampus (41).

Besides the ribosome, our translation reactions utilize many accessory enzymes such as elongation factors and aminoacyl-tRNA synthetases that also have divalent cation requirements. Therefore, both Mn^{2+} and Fe^{2+} may be fully functional ribosomal substitutes with different effectiveness caused by lower activity of one or more of these accessory enzymes. Indeed, the relative activity of arginine t-RNA synthetase and myokinase are both lower with Mn^{2+} or Fe^{2+} than with Mg^{2+} (42, 43).

While intracellular Mg^{2+} is consistently 10^{-3} M in cellular life (44), specific physiological or environmental conditions can significantly elevate intracellular Fe^{2+} and Mn^{2+}. Under oxidative stress, some microbes accumulate excess Mn^{2+} (e.g. radiation-tolerant *Deinococcus radiodurans* contains ~10 times higher Mn^{2+} than *E. coli* (~10^{-5} M Mn^{2+} (45, 46))). In the absence of oxygen, *E. coli* contains ~10 times higher labile Fe^{2+} (~10^{-4} M) than when grown with oxygen (~10^{-5} M (47)). Thus, it is possible that the absence of Fe^{2+} and Mn^{2+} in experimentally determined ribosomal structures is reflective of culturing and purification conditions (high O_2, high Mg^{2+}, low Fe^{2+}, and low Mn^{2+}), and that other cations may also be present under diverse physiological conditions.

We have shown that the translation system functions with mixtures of divalent cations, which are variable during long-term evolutionary processes and during short term changes in bioavailability and oxidative stress. When combined with previous results that DNA replication and transcription can be facilitated by Fe^{2+} and Mn^{2+} (16-23, 36, 37), our findings that Fe^{2+} can mediate rRNA folding and that both Fe^{2+} and Mn^{2+}

bioRxiv preprint doi: https://doi.org/10.1101/256958; this version posted July 6, 2018. The copyright holder for this preprint (which was not certified by peer review) is the author/funder. All rights reserved. No reuse allowed without permission.

can support translation of active protein has revealed that these prebiotically relevant metals can facilitate the entire central dogma of molecular biology (DNA→RNA→protein). These findings raise important questions about evolutionary and physiological roles for Fe^{2+} and Mn^{2+} in ancient and extant biological systems. Were Mg^{2+}, Fe^{2+} and Mn^{2+} collaborators as cofactors on the ancient Earth, when Fe^{2+} and Mn^{2+} were more abundant (1-5), and Mg^{2+} was less abundant (2), than today? What was the role of Fe^{2+} and Mn^{2+} in the origin and early evolution of the translational system? Finally, what are the implications for ribosome-bound Fe^{2+} in oxidative damage and disease?

Materials and Methods

rRNA folding via SHAPE. SHAPE methods were adapted from previously published protocols (29) using the intact ~2900 nt *Thermus thermophilus* 23 rRNA (LSU) in the presence of 250 mM Na^+, which favors formation of secondary structure, and in 250 mM Na^+ plus a divalent cation (10 mM Mg^{2+} or 2.5 mM Fe^{2+}, both as chloride salts) to favor formation of tertiary interactions. Adaptations were made to facilitate folding and N-methylisatoic anhydride modification of RNA in an anoxic chamber under a 98% Ar and 2% H_2 atmosphere. To keep rRNA samples oxygen-free, rRNA samples in 200 mM NaOAc, 50 mM NaHEPES (pH 8) were lyophilized, transferred into the anoxic chamber, and rehydrated with nuclease-free, degassed water. After rRNA modification, as described in ref. (29), divalent cations were extracted from the rRNA by chelating beads. Samples were then removed from the anoxic chamber for analysis by capillary electrophoresis (29). Nucleotides were classified as exhibiting a significant change in SHAPE reactivity if either the original reactivity (in Na^+) or final reactivity (in Na^+/Mg^{2+} or Na^+/Fe^{2+}) was >0.3 SHAPE units. To compare the Fe^{2+}- and Mg^{2+}-responsiveness of specific nucleotides, we binned nucleotides into three categories (increased, decreased, or little/no change) based on their general SHAPE reactivity response to each divalent cation (SHAPE data are found in **Additional Data Table S1**).

***In vitro* translation.** Each 30 µL reaction contained 2 µM (4.5 µL of 13.3 µM stock) *E. coli* ribosomes in 10 mM Mg^{2+} (New England Biolabs, Ipswich MA, USA; catalog # P0763S), 3 µL factor mix (with RNA polymerase, and transcription/translation factors in 10 mM Mg^{2+}) from the PURExpress® Δ Ribosome Kit (New England Biolabs E3313S), 0.1 mM amino acid mix (Promega, Madison WI, USA; catalog # L4461), and 0.2 mM tRNAs from *E. coli* MRE 600 (Sigma-Aldrich, St. Louis MO, USA; product # TRNAMRE-RO). Thus, a total of 2.5 mM "background" Mg^{2+} was present in each reaction (**Fig. S1a**). To remove the background Mg^{2+}, we exchanged the buffer of the ribosome and factor mix using centrifugal filter units. Thirty microliters of either ribosome solution or factor mix was added to an Amicon Ultra 0.5 mL centrifugal filter (Millipore-Sigma), followed by 450 µL of divalent-free buffer (20 mM HEPES pH 7.6, 30 mM KCl, and 7 mM β-mercaptoethanol). Samples where spun at 14,000 x g at 4°C until the minimum sample volume (~15 µL) was reached. The samples were resuspended in 450 µL of divalent-free buffer and centrifugation was repeated. The samples were then transferred to new tubes and 15 µL of divalent-free buffer was added to bring the volume to 30 µL. This process decreased Mg^{2+} concentrations in the ribosome and factor mix from 10 mM to 10-30 µM Mg^{2+}, resulting in 4-6 µM Mg^{2+} in each reaction (**Fig. S1b, S1c)**.

Translation reaction buffer. The reaction buffer was based on Shimizu et al. (48), with HEPES-OH instead of phosphate buffer to avoid precipitation of metal phosphates. We found that rates of translation were consistently lower with Tris-HCl than HEPES-OH, and therefore HEPES-OH was used as the buffer for all experiments. Buffer consisted of 20 mM HEPES-OH (pH 7.3), 95 mM potassium glutamate, 5 mM NH_4Cl, 0.5 mM $CaCl_2$, 1 mM spermidine, 8 mM putrescine, 1 mM dithiothreitol (DTT), 2 mM adenosine triphosphate (ATP), 2 mM guanosine triphosphate (GTP), 1 mM uridine triphosphate (UTP), 1 mM cytidine triphosphate (CTP), 10 mM creatine phosphate (CP), and 53 µM 10-formyltetrahydrofolate. The reaction buffer was lyophilized and stored at -80°C until resuspension in anoxic nuclease-free water immediately before experiments in an anoxic chamber.

bioRxiv preprint doi: https://doi.org/10.1101/256958; this version posted July 6, 2018. The copyright holder for this preprint (which was not certified by peer review) is the author/funder. All rights reserved. No reuse allowed without permission.

Translation experimental conditions. All reactions (30 μL total volume) were assembled and incubated in the anoxic chamber. All divalent cation salts used in experiments ($MgCl_2$, $FeCl_2$, $MnCl_2$, $Zn(OAc)_2$, $CoCl_2$, $CuSO_4$) were added to 7 mM final concentration, with the exception of $MgCl_2$ and $FeCl_2$, which were tested over a range of final concentrations (1, 3, 4, 5, 6, 7, 8, 9, and 11 mM; **Fig. S1**). Solutions were clear, with no indication of metal precipitate, suggesting that reduced, divalent metals cations were the primary chemical species. All experiments were assembled in the following order: dihydrofolate reductase (DHFR) mRNA (~5 μg per 30 μL reaction; see **Supplemental Information** for more details), factor mix, ribosomes, amino acids, tRNA, nuclease-free H_2O, reaction buffer. Changing the order of reactant addition did not affect translational activity. Reactions were run in triplicate on a 37°C heat block for up to 120 minutes. Reactions were quenched on ice and stored on ice until they were assayed for protein synthesis.

Protein activity assay. Protein synthesis was measured using a DHFR assay kit (Sigma-Aldrich product # CS0340), which measures the oxidation of NADPH (60 mM) to $NADP^+$ by dihydrofolic acid (51 μM). Assays were performed by adding 5 μL of protein synthesis reaction to 995 μL of 1x assay buffer. The NADPH absorbance peak at 340 nm (Abs_{340}) was measured in 15 s intervals over 2.5 min. The slope of the linear regression of Abs_{340} vs. time was used to determine protein activity (Abs_{340} min^{-1}). Different counter ions (Cl^-, CH_3COO^-, SO_4^{2-}) had no effect on protein synthesis from mRNA. To our knowledge, no dependence on, nor inhibitory effect of Mg^{2+} or Fe^{2+} exists for DHFR. We confirmed this by varying the amounts of metals in our assay reaction, which had no effect on DHFR activity (data not shown).

Ribosome metal content. The Fe and Mn content of *E. coli* ribosomes was measured by total reflection x-ray fluorescence (TRXF) spectroscopy after the ribosomes were incubation in 7 mM $FeCl_2$ or 7 mM $MnCl_2$. Detailed methods are provided in the **Supplemental Information**.

Quantum mechanical calculations. The atomic coordinates of a Mg^{2+}-rRNA clamp were initially extracted from the X-ray structure of the *Haloarcula marismortui* large ribosomal subunit (PDB 1JJ2) (49). The free 5′ and 3′ termini of the phosphate groups were capped with methyl groups in lieu of the remainder of the RNA polymer, and hydrogen atoms were added, where appropriate (**Fig. S3**). The details of calculations were adapted from previous publications (11, 19) and are provided in the **Supplemental Information**.

ACKNOWLEDGMENTS. This research was supported by the National Aeronautics and Space Administration grants NNX14AJ87G, NNX16AJ28G, and NNX16AJ29G. We acknowledge helpful discussions with Corinna Tuckey of New England Biolabs, and with Eric B. O'Neill and Claudia Montllor Albalate of Georgia Institute of Technology. We thank Michael Goodisman for access to a capillary electrophoresis instrument.

Competing interests. The authors declare that they have no competing interests with the contents of this article.

Author contributions: MSB, TKL, JCB, ARR, NVH, LDW, and JBG conceived and designed the experiments. MSB and TKL collected data and performed analysis. ASP contributed analysis. MSB, TKL, LDW, and JBG wrote the paper with editorial input from all authors.

References

1. Derry LA (2015) Causes and consequences of mid-Proterozoic anoxia. *Geophys. Res. Lett.* 42(20):8538-8546.
2. Jones C, Nomosatryo S, Crowe SA, Bjerrum CJ, & Canfield DE (2015) Iron oxides, divalent cations, silica, and the early earth phosphorus crisis. *Geology* 43(2):135-138.
3. Poulton SW & Canfield DE (2011) Ferruginous conditions: a dominant feature of the ocean through Earth's history. *Elements* 7(2):107-112.

bioRxiv preprint doi: https://doi.org/10.1101/256958; this version posted July 6, 2018. The copyright holder for this preprint (which was not certified by peer review) is the author/funder. All rights reserved. No reuse allowed without permission.

4. Holland HD (1984) *The Chemical Evolution of the Atmosphere and Oceans* (Princeton University Press, Princeton, N.J.).
5. Johnson JE, Webb SM, Ma C, & Fischer WW (2016) Manganese mineralogy and diagenesis in the sedimentary rock record. *Geochem. Cosmochim. Acta* 173:210-231.
6. Ramakrishnan V (2002) Ribosome structure and the mechanism of translation. *Cell* 108(4):557-572.
7. Fox GE (2010) Origin and evolution of the ribosome. *Cold Spring Harb. Perspect.* 2(9):a003483.
8. Bernier CR, Petrov AS, Kovacs NA, Penev PI, & Williams LD (2018) Translation: The Universal Structural Core of Life. *Mol Biol Evol*:10.1093/molbev/msy1101.
9. Klein DJ, Moore PB, & Steitz TA (2004) The contribution of metal ions to the structural stability of the large ribosomal subunit. *RNA* 10(9):1366-1379.
10. Cusack S (1997) Aminoacyl-tRNA synthetases. *Curr. Opin. Struct. Biol.* 7(6):881-889.
11. Petrov AS, Bowman JC, Harvey SC, & Williams LD (2011) Bidentate RNA–magnesium clamps: On the origin of the special role of magnesium in RNA folding. *RNA* 17(2):291-297.
12. Hsiao C & Williams LD (2009) A recurrent magnesium-binding motif provides a framework for the ribosomal peptidyl transferase center. *Nucleic Acid Res.* 37(10):3134-3142.
13. Schuwirth BS*, et al.* (2005) Structures of the bacterial ribosome at 3.5 Å resolution. *Science* 310(5749):827-834.
14. Demeshkina N, Jenner L, Westhof E, Yusupov M, & Yusupova G (2012) A new understanding of the decoding principle on the ribosome. *Nature* 484(7393):256-259.
15. Selmer M*, et al.* (2006) Structure of the 70S ribosome complexed with mRNA and tRNA. *Science* 313(5795):1935-1942.
16. Pyle A (2002) Metal ions in the structure and function of RNA. *J. Biol. Inorg. Chem.* 7(7):679-690.
17. Pyle AM (1993) Ribozymes: a distinct class of metalloenzymes. *Science* 261(5122):709-714.
18. Ward WL, Plakos K, & DeRose VJ (2014) Nucleic acid catalysis: metals, nucleobases, and other cofactors. *Chem. Rev.* 114(8):4318-4342.
19. Athavale SS*, et al.* (2012) RNA folding and catalysis mediated by iron (II). *PLoS One* 7(5):e38024.
20. Popović M, Fliss PS, & Ditzler MA (2015) *In vitro* evolution of distinct self-cleaving ribozymes in diverse environments. *Nucleic Acids Res.* 43(14):7070-7082.
21. Okafor CD*, et al.* (2017) Iron mediates catalysis of nucleic acid processing enzymes: support for Fe (II) as a cofactor before the great oxidation event. *Nucleic Acids Res.* 45(7):3634-3642.
22. Tabor S & Richardson CC (1989) Effect of manganese ions on the incorporation of dideoxynucleotides by bacteriophage T7 DNA polymerase and *Escherichia coli* DNA polymerase I. *Proc. Natl. Acad. Sci.* 86(11):4076-4080.
23. Litman RM (1971) The differential effect of magnesium and manganese ions on the synthesis of poly (dGd· C) and *Micrococcus luteus* DNA by *Micrococcus luteus* DNA polymerase. *J. Mol. Biol.* 61(1):1-23.
24. Dann III CE*, et al.* (2007) Structure and mechanism of a metal-sensing regulatory RNA. *Cell* 130(5):878-892.
25. Mortimer SA & Weeks KM (2007) A fast-acting reagent for accurate analysis of RNA secondary and tertiary structure by SHAPE chemistry. *J. Am. Chem. Soc.* 129(14):4144-4145.
26. Athavale SS*, et al.* (2012) Domain III of the *T. thermophilus* 23S rRNA folds independently to a near-native state. *RNA* 18(4):752-758.
27. Hsiao C*, et al.* (2013) Molecular paleontology: a biochemical model of the ancestral ribosome. *Nucleic Acids Research* 41(5):3373-3385.
28. Lanier KA, Athavale SS, Petrov AS, Wartell R, & Williams LD (2016) Imprint of ancient evolution on rRNA folding. *Biochemistry* 55(33):4603-4613.
29. Lenz TK, Norris AM, Hud NV, & Williams LD (2017) Protein-free ribosomal RNA folds to a near-native state in the presence of Mg^{2+}. *RSC Adv.* 7(86):54674-54681.

bioRxiv preprint doi: https://doi.org/10.1101/256958; this version posted July 6, 2018. The copyright holder for this preprint (which was not certified by peer review) is the author/funder. All rights reserved. No reuse allowed without permission.

30. Takanami M & Okamoto T (1963) Interaction of ribosomes and synthetic polyribonucleotides. *J. Mol. Biol.* 7(4):323-333.
31. Kigawa T*, et al.* (1999) Cell-free production and stable-isotope labeling of milligram quantities of proteins. *FEBS Lett.* 442(1):15-19.
32. Goldberg A (1966) Magnesium binding by *Escherichia coli* ribosomes. *J. Mol. Biol.* 15(2):663-673.
33. Pronczuk A, Baliga B, & Munro H (1968) Effect of nucleoside triphosphate and magnesium ion concentration on the stability and function of rat liver polysomes *in vitro*. *Biochem. J.* 110(4):783-788.
34. Brion P & Westhof E (1997) Hierarchy and dynamics of RNA folding. *Annu. Rev. Biophys. Biomol. Struct.* 26:113-137.
35. Tinoco I, Jr. & Bustamante C (1999) How RNA folds. *J. Mol. Biol.* 293(2):271-281.
36. Bock CW, Katz AK, Markham GD, & Glusker JP (1999) Manganese as a replacement for magnesium and zinc: functional comparison of the divalent ions. *J. Amer. Chem. Soc.* 121(32):7360-7372.
37. Imlay JA (2014) The mismetallation of enzymes during oxidative stress. *J. Biol. Chem.* 289(41):28121-28128.
38. Zheng H, Shabalin IG, Handing KB, Bujnicki JM, & Minor W (2015) Magnesium-binding architectures in RNA crystal structures: validation, binding preferences, classification and motif detection. *Nucleic Acids Res.* 43(7):3789-3801.
39. Bowman JC, Lenz TK, Hud NV, & Williams LD (2012) Cations in charge: magnesium ions in RNA folding and catalysis. *Curr. Opin. Struct. Biol.* 22(3):262-272.
40. Hensley MP, Tierney DL, & Crowder MW (2011) Zn (II) binding to Escherichia coli 70S ribosomes. *Biochemistry* 50(46):9937-9939.
41. Honda K*, et al.* (2005) Ribosomal RNA in Alzheimer disease is oxidized by bound redox-active iron. *J. Biol. Chem.* 280(22):20978-20986.
42. Craine J & Peterkofsky A (1976) Studies on arginyl-tRNA synthetase from *Escherichia coli* B. Dual role of metals in enzyme catalysis. *J. Biol. Chem.* 251(1):241-246.
43. Ito Y, Tomasselli AG, & Noda LH (1980) ATP: AMP phosphotransferase from baker's yeast: purification and properties. *Eur. J. Biochem.* 105(1):85-92.
44. Da Silva JF & Williams RJP (2001) *The Biological Chemistry of the Elements: the Inorganic Chemistry of Life* (Oxford University Press) Second Ed.
45. Daly MJ*, et al.* (2004) Accumulation of Mn(II) in *Deinococcus radiodurans* facilitates gamma-radiation resistance. *Science* 306(5698):1025-1028.
46. Outten CE & O'Halloran TV (2001) Femtomolar sensitivity of metalloregulatory proteins controlling zinc homeostasis. *Science* 292(5526):2488-2492.
47. Beauchene NA*, et al.* (2017) O2 availability impacts iron homeostasis in *Escherichia coli*. *Proc. Natl. Acad. Sci.* 14 (46):12261-12266.
48. Shimizu Y*, et al.* (2001) Cell-free translation reconstituted with purified components. *Nature Biotechnol.* 19(8):751.
49. Ban N, Nissen P, Hansen J, Moore PB, & Steitz TA (2000) The complete atomic structure of the large ribosomal subunit at 2.4 Å resolution. *Science* 289(5481):905-920.
50. Keedy HE, Thomas EN, & Zaher HS (2018) Decoding on the ribosome depends on the structure of the mRNA phosphodiester backbone. *Proc Natl Acad Sci*:DOI: 10.1073/pnas.1721431115.
51. Kjeldgaard M, Nissen P, Thirup S, & Nyborg J (1993) The crystal structure of elongation factor EF-Tu from *Thermus aquaticus* in the GTP conformation. *Structure* 1(1):35-50.
52. Campuzano S & Modolell J (1981) Effects of antibiotics, N-Acetylaminoacyl-tRNA and other agents on the Elongation-Factor-Tu dependent and ribosome-dependent GTP hydrolysis promoted by 2′(3′)-O-l-Phenylalanyladenosine. *Eur. J. Biochem.* 117(1):27-31.
53. Chen Y, Feng S, Kumar V, Ero R, & Gao Y-G (2013) Structure of EF-G–ribosome complex in a pretranslocation state. *Nature Struct. Mol. Biol.* 20(9):1077.

bioRxiv preprint doi: https://doi.org/10.1101/256958; this version posted July 6, 2018. The copyright holder for this preprint (which was not certified by peer review) is the author/funder. All rights reserved. No reuse allowed without permission.

54. Lovgren TNE, Heinonen J, & Loftfield RB (1978) Mechanism of aminoacylation of transfer ribonucleic-acid. Role of magnesium and spermine in synthesis of isoleucyl-transfer RNA. *J. Biol. Chem.* 253(19):6702-6710.
55. Thiebe R (1975) Aminoacylation of tRNA. Magnesium requirement and spermidine effect. *FEBS Lett.* 51(1-2):259-261.
56. Blanquet S, Dessen P, & Kahn D (1984) Properties and specificity of methionyl-tRNAfMet formyltransferase from *Escherichia coli*. *Methods Enzymol.* 106:141-152.
57. Morin L (1977) Creatine kinase: stability, inactivation, reactivation. *Clin. Chem.* 23(4):646-652.
58. Vasavada K, Kaplan J, & Rao BN (1984) Analysis of phosphorus-31 NMR spectra of enzyme-bound reactants and products of adenylate kinase using density matrix theory of chemical exchange. *Biochemistry* 23(5):961-968.
59. Munoz-Dorado J, Inouye S, & Inouye M (1990) Nucleoside diphosphate kinase from *Myxococcus xanthus*. II. Biochemical characterization. *J. Biol. Chem.* 265(5):2707-2712.
60. Kankare J*, et al.* (1994) The structure of *E. coli* soluble inorganic pyrophosphatase at 2.7 Å resolution. *Protein Eng. Des. Sel.* 7(7):823-830.
61. Bloch-Frankenthal L (1954) The role of magnesium in the hydrolysis of sodium pyrophosphate by inorganic pyrophosphatase. *Biochem. J.* 57(1):87.
62. Bernier CR*, et al.* (2014) RiboVision suite for visualization and analysis of ribosomes. *Faraday Disc* 169:195-207.

bioRxiv preprint doi: https://doi.org/10.1101/256958; this version posted July 6, 2018. The copyright holder for this preprint (which was not certified by peer review) is the author/funder. All rights reserved. No reuse allowed without permission.

Table 1. Structural and functional roles for select divalent cations in the translation system. All biomolecules in the table have been shown to require Mg^{2+} and may also be active with Fe^{2+} or Mn^{2+}. "n.a." indicates that data are not available.

Translation system component(s)	Location of divalent ion	Role of divalent cation	Optimal $[Mg^{2+}]$ (mM)
Ribosome			
LSU/SSU	M^{2+}-rRNA clamps (11)	Mediates and maintains folding/structure of rRNAs	~10 (31)
LSU	Dinuclear microclusters (12)	Frames peptidyl transferase center (PTC)	~10 (31)
LSU/SSU	LSU/SSU interface (24)	Mediates docking of mRNA to SSU and association of SSU with LSU	~10 (31)
SSU/mRNA	Critical bend in mRNA between the P-site and A-site codons (15, 50)	Maintains correct reading frame mRNA	~10 (31)
A-site tRNA/ P-site tRNA	tRNA-tRNA interface (24)	Stabilize tRNAs in the PTC	~10 (31)
LSU/tRNA	rRNA-tRNA interface (24)	Stabilize rRNA-tRNA in the PTC	~10 (31)
Auxiliary			
EF-Tu	GTP binding site (51)	Stabilizes the transition state	5-15 (52)
EF-G	GTP binding site (53)	Stabilizes the transition state	n.a.
Aminoacyl-tRNA synthetases	ATP binding site (54)	Stabilizes the transition state	>1 (55)
Methionyl-tRNA transformylase	ATP binding site (56)	Stabilizes the transition state	7 (56)
Creatine kinase	NTP binding site (57)	Stabilizes the transition state	~5 (57)
Myokinase	Acceptor NDP binding site (58)	Stabilizes the transition state	~3 (43)
Nucleoside-diphosphate kinase	NTP binding site (59)	Stabilizes the transition state	>1
Pyrophosphatase	Active site (60)	Stabilizes the transition state	>7 (61)

396

bioRxiv preprint doi: https://doi.org/10.1101/256958; this version posted July 6, 2018. The copyright holder for this preprint (which was not certified by peer review) is the author/funder. All rights reserved. No reuse allowed without permission.

Figure Legends

Fig. 1. Divalent cations serve many structural and functional roles in the ribosome. Mg^{2+} ions: **a)** form bidentate clamps with adjacent phosphate groups of rRNA (beige carbon atoms), **b)** form dinuclear microclusters that frame the rRNA of the peptidyl transferase center, **c)** stabilize the LSU-SSU interface, **d)** stabilize a functional kink in mRNA (green), **e)** stabilize association of tRNA (teal) with 23S rRNA, and **f)** stabilize association of mRNA with 16S rRNA. Thick dashed lines are first shell RNA interactions of Mg^{2+}. Dotted lines indicate second shell interactions. Images are of the *Thermus thermophilus* ribosome (PDB ID: 1VY4) because the structural information available for *T. thermophilus* ribosomes is more accurate than for *E. coli*. This figure was generated with the program RiboVision (62).

Fig. 2. SHAPE reactivities mapped onto the LSU rRNA secondary structure in **a)** Na^{+}, **b)** Na^{+}/Fe^{2+}, or **c)** Na^{+}/Mg^{2+}. Key functional elements are labeled in panel a, and the scale in panel (a) applies to panels b and c. **d)** Fe^{2+}-induced changes (ΔFe^{2+}) in SHAPE reactivity calculated by subtracting Na^{+} data from Na^{+}/Fe^{2+} data for each nucleotide, and **e)** Mg^{2+}-induced changes (ΔMg^{2+}) in SHAPE reactivity calculated by subtracting Na^{+} data from Na^{+}/Mg^{2+} data for each nucleotide. The scale shown for panel d also applies to panel e. Positive values indicate increased SHAPE reactivity in presence of the divalent cation, while negative values denote decreased reactivity. Regions where data are not available (5' and 3' ends) are grey. These figures were generated with the program RiboVision (62). *Thermus thermophilus* rRNA was used as the analytical model for SHAPE experiments because the structural information is more accurate than for *E. coli*. The L11 binding region, where the greatest discrepancy between Fe^{2+} and Mg^{2+} is observed, is indicated with an arrow.

Fig. 3. Mg^{2+} and Fe^{2+} stimulate translational activity over a range of concentrations. The activity of the translation product (dihydrofolate reductase, which catalyzes the oxidation of NADPH, with a maximum absorbance at 340 nm) was used as a proxy for protein production. Translation reactions were run for 120 minutes. All translation reactions contained 2.5 mM background Mg^{2+}, to which varying amounts of additional Mg^{2+} or Fe^{2+} were added. The error bars for triplicate experiments (N=3) are plotted as the standard error of the mean.

Fig. 4. Fe^{2+} consistently supports 50-80% of the translational activity as Mg^{2+} when the translation experiments are run for 15-120 minutes. The activity of the translation product (dihydrofolate reductase, which catalyzes the oxidation of NADPH, with a maximum absorbance at 340 nm) was used as a proxy for protein production. All translation reactions contained 2.5 mM background Mg^{2+}, to which 7 mM additional Mg^{2+} or Fe^{2+} were added, totaling to 9.5 mM divalent cation. The error bars for triplicate experiments (N=3) are plotted as the standard error of the mean.

Fig. 5. Mn^{2+} can support translation after removal of background Mg^{2+}. **a)** Reactions prepared with washed *E. coli* ribosomes, reducing the background Mg^{2+} to 1 mM, to which 7, 9, or 11 mM additional Mg^{2+}, Fe^{2+}, or Mn^{2+} were added, totaling 8, 10, or 12 mM divalent cation (M^{2+}). **b)** Reactions prepared using washed *E. coli* ribosomes and washed factor mix, which reduced the background Mg^{2+} to the low µM level, to which 8, 10, or 12 mM additional, Mg^{2+}, Fe^{2+}, or Mn^{2+} were added. The activity of the translation product (dihydrofolate reductase, which catalyzes the oxidation of NADPH, with a maximum absorbance at 340 nm) was used as a proxy for protein production. The error bars for triplicate experiments (N=3) are plotted as the standard error of the mean.

a) Mg^{2+}-rRNA clamp

b) dinuclear microcluster

c) LSU-SSU interface

d) mRNA bend

e) rRNA-tRNA interface

f) rRNA-mRNA interface

bioRxiv preprint doi: https://doi.org/10.1101/256958; this version posted July 6, 2018. The copyright holder for this preprint (which was not certified by peer review) is the author/funder. All rights reserved. No reuse allowed without permission.

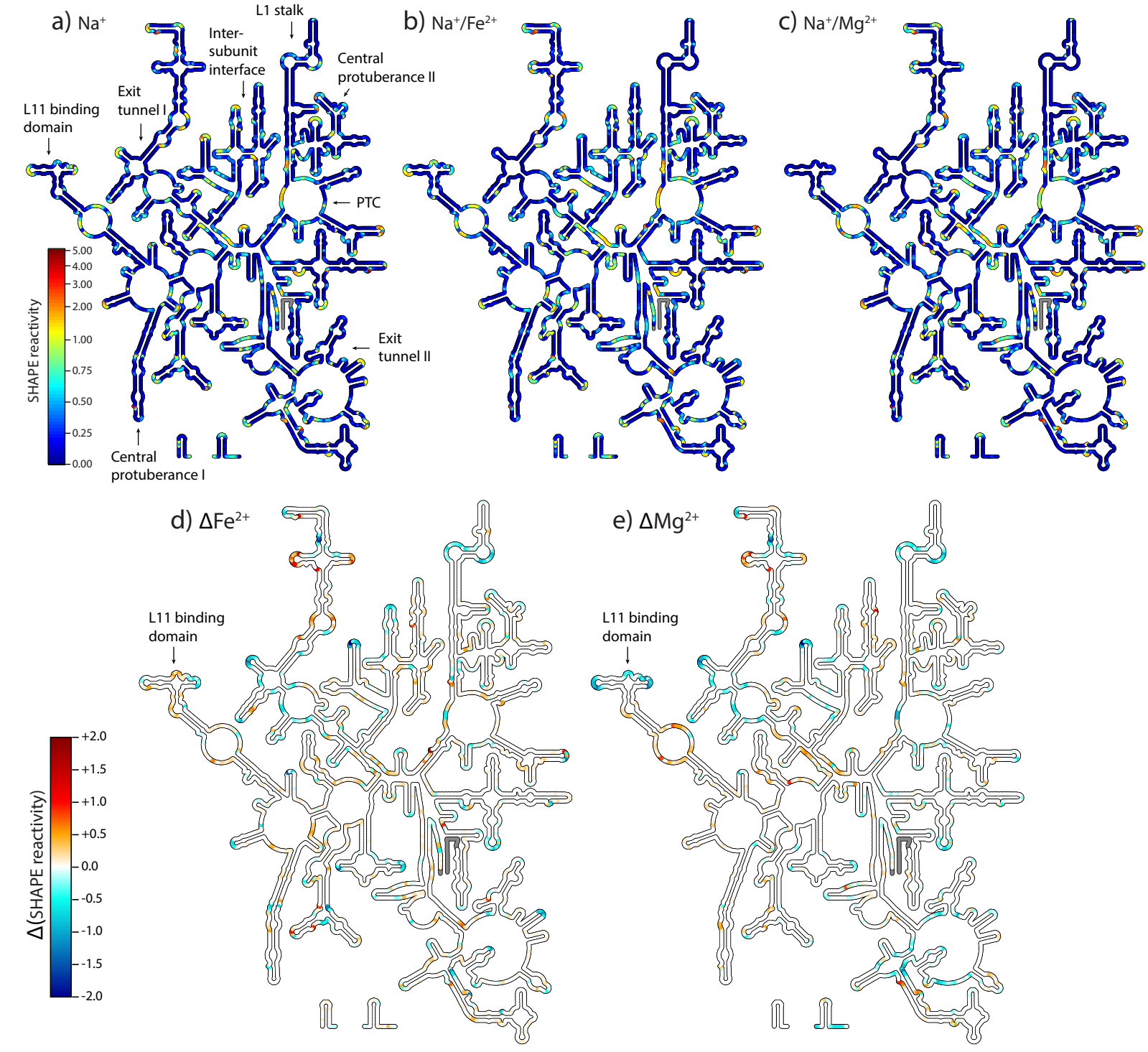
a) Na+
L1 stalk
Inter-subunit interface
Central protuberance II
Exit tunnel I
L11 binding domain
PTC
Exit tunnel II
Central protuberance I
SHAPE reactivity
5.00
4.00
3.00
2.00
1.00
0.75
0.50
0.25
0.00
b) Na+/Fe2+
c) Na+/Mg2+
d) ΔFe2+
L11 binding domain
e) ΔMg2+
L11 binding domain
Δ(SHAPE reactivity)
+2.0
+1.5
+1.0
+0.5
0.0
-0.5
-1.0
-1.5
-2.0

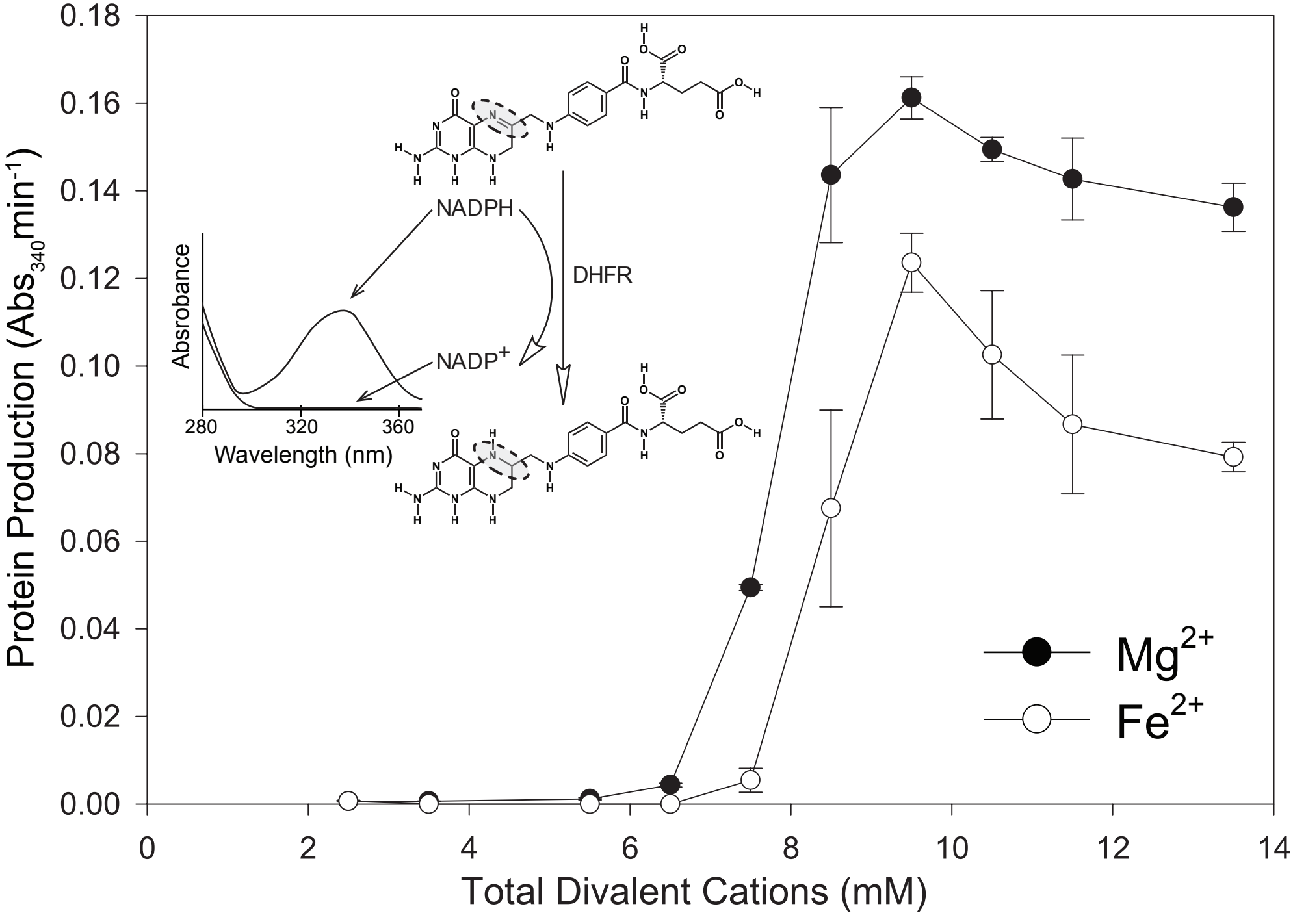
Protein Production (Abs340min-1)
0.18
0.16
0.14
0.12
0.10
0.08
0.06
0.04
0.02
0.00
0
2
4
6
8
10
12
14
Total Divalent Cations (mM)
NADPH
DHFR
NADP+
Absrobance
280
320
360
Wavelength (nm)
Mg2+
Fe2+

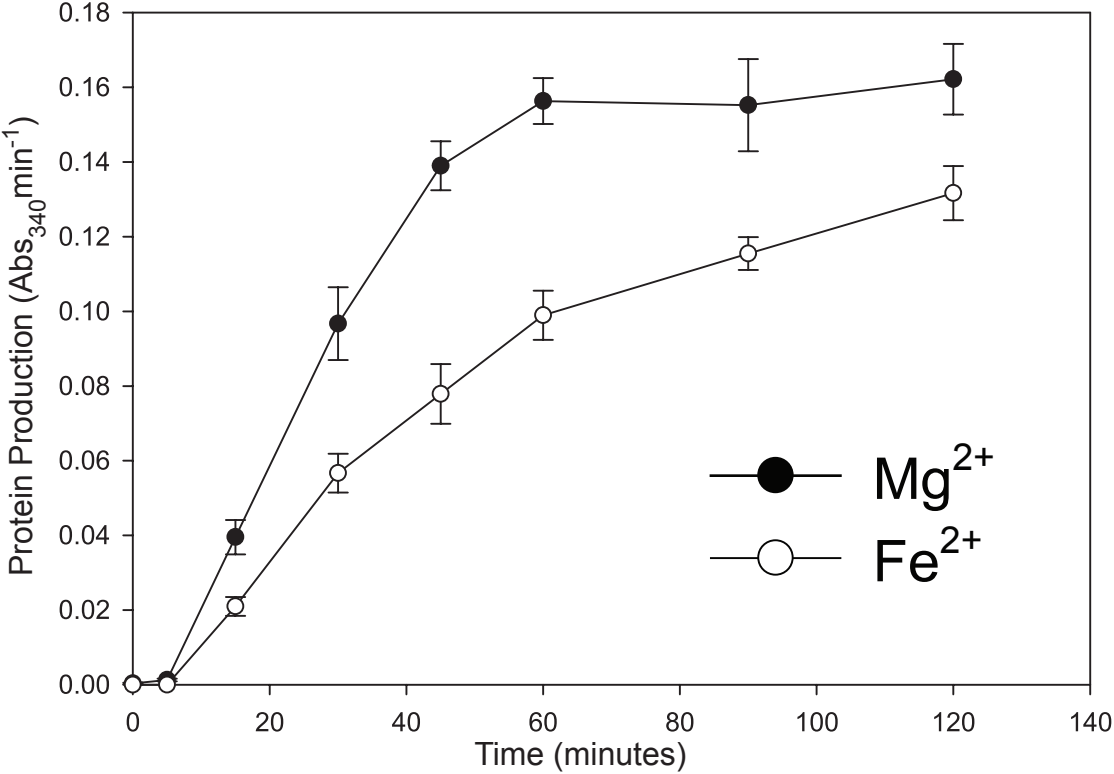
0.18
0.16
0.14
0.12
0.10
0.08
0.06
0.04
0.02
0.00
Protein Production (Abs340min-1)
0
20
40
60
80
100
120
140
Time (minutes)
Mg2+
Fe2+

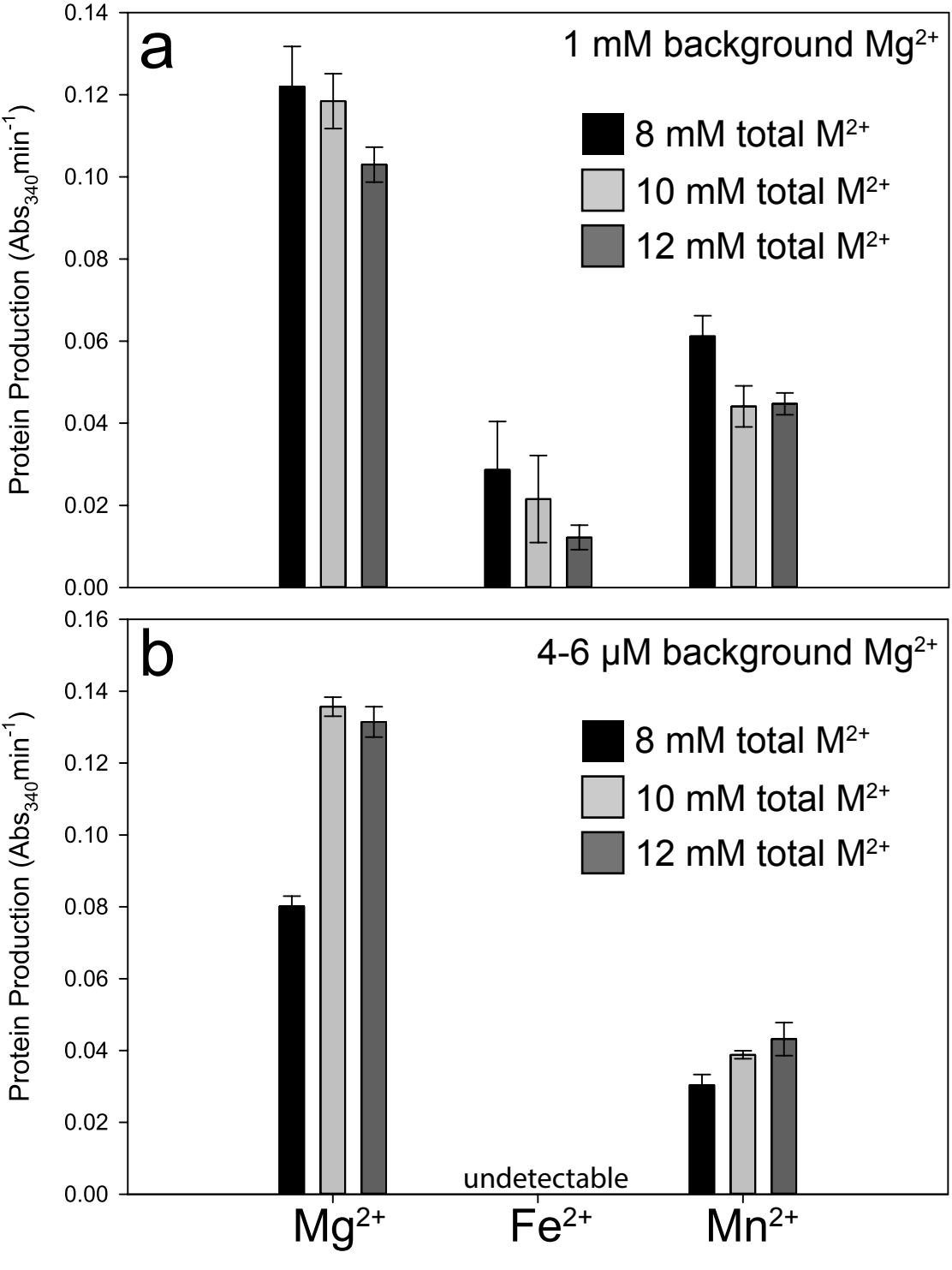
a
1 mM background Mg2+
8 mM total M2+
10 mM total M2+
12 mM total M2+
Protein Production (Abs340min-1)
0.14
0.12
0.10
0.08
0.06
0.04
0.02
0.00
b
4-6 µM background Mg2+
8 mM total M2+
10 mM total M2+
12 mM total M2+
Protein Production (Abs340min-1)
0.16
0.14
0.12
0.10
0.08
0.06
0.04
0.02
0.00
undetectable
Mg2+
Fe2+
Mn2+